Magnetic Actuation for Full Dexterity Micro-Robotic Control Using Rotating Permanent Magnets

Patrick Ryan and Eric Diller

Abstract—Recent work in magnetically-actuated micro-scale robots for biomedical or microfluidic applications has resulted in magnetic actuation systems which can remotely command precise five-degree-of-freedom control of magnetic devices. This paper presents a new type of actuation system which uses an array of rotating permanent magnets to generate the same level of control over untethered micro-scale devices with the potential for increased field and gradient strength and minimal heat generation. In contrast with previous permanent magnet actuation systems, the system proposed here does not require any hazardous translational motion of the control magnets, resulting in a simple, safe, and inexpensive system. The proof-of-concept prototype system presented, with eight permanent magnets, can create fields and field gradients in any direction with variable magnitudes between zero and 30 mT and 0.83 Tm^{-1}, respectively. The effectiveness of the system is shown through characterization and feedback control of a 250 µm micro-magnet in a 3D path-following task with average accuracy of 25 µm. An optimization framework is presented for designing system configurations for targeted applications.

Index Terms—Magnetic manipulation, micromanipulator, micro-robot, untethered

I. INTRODUCTION

The wireless control of small-scale robotic devices is an exciting prospect due to the ability of these devices to access enclosed spaces such as those within the human body. The use of externally-generated magnetic fields has been shown to be a preferred method of control for untethered devices that range in size from micrometers to centimeters when physical tethers to the device are not possible. This type of magnetic control is suitable for wireless operation of devices in confined spaces, and therefore has many medical applications [1],[2] including ophthalmic procedures [3], catheter steering [4],[5], and wireless capsule endoscopy [6],[7] as well as applications in micro-object manipulation including single cells [8], and micro-particles [9].

For many applications involving wireless magnetic actuation, a high level of control of the position and orientation of the micro-device is required. An implement containing a single magnetic dipole can be positioned with a maximum of five-degrees-of-freedom (DOF), consisting of three translational DOF and two rotational DOF. An established method for achieving 5-DOF control of a single

magnetic device uses electromagnetic coils to produce the required magnetic fields and field gradients [3],[10]. Full 6-DOF control is possible but requires the controlled device to have a more complex magnetization profile which may limit its utility for practical applications [11]. For electromagnetic systems, another control capability with similar field generation requirements is simultaneous control of multiple microrobots in two or three-dimensions [12], [13].

An alternative method for field generation is to use permanent magnets instead of electromagnetic coils. Both electromagnets and permanent magnets generate an equivalent magnetic field, however, the use of electromagnetics has often been the preferred technique due to the ability to rapidly control the field strength by changing the coil current. This enables high frequency field modulation, and the ability to turn off the field completely. Electromagnetic systems, however, are limited in that the high current required for strong field generation results in a significant temperature rise within the coils due to Joule heating. This heating often requires active cooling solutions, and can result in increased workplace temperature, making this type of system undesirable for heat-sensitive applications such as biomedical procedures involving cells. If permanent magnets are instead used as the field source, the field is produced using no input power, resulting in no heat generation near the workspace. Additionally, relative to electromagnetic devices, permanent magnet systems are able to generate stronger fields and field gradients by a factor of approximately 10 to 20, and 2 to 3, respectively, depending on the size of the workspace [14]. An increase in field and gradient strength allows agents to be driven faster [15]-[17] and many applications are field or gradient limited.

Permanent magnet systems have previously been shown to be capable of providing 4-DOF control of a capsule endoscope by using a hand-held [19] or robotically actuated [20],[21] permanent magnet positioned outside the body. The Stereotaxis Niobe system uses permanent magnets for catheter steering and is currently in clinical use [4]. Most recently, a permanent magnet system has been shown to be capable of 5-DOF control of a capsule endoscope using a single permanent magnet positioned and oriented above the workspace using a robotic manipulator [6]. This method has demonstrated the highest level of control for a permanent magnet system but downsides of this approach include the potential hazard of the mobile robotic manipulator, the high cost of the system, and the inability to independently control the field magnitude. Similarly, the system shown by Zhang et al. [22] uses an array of continuously rotating magnets, positioned symmetrically around the workspace for simple and safe field production, although this system is limited to producing only in-plane, uniform, rotating magnetic fields.

P. Ryan and E. Diller are with the department of Mechanical and Industrial Engineering, University of Toronto, Toronto, Canada, M5S 3G8
(e-mail: pryan@mie.utoronto.ca; ediller@mie.utoronto.ca)

In this paper, we propose a new method to achieve full 5-DOF control which uses permanent magnets that rotate in place. Unlike a robotically-manipulated single magnet system such as that shown in [6], the proposed system is composed of multiple permanent magnets, each with the ability to be rotated independently of the other magnets. This system configuration is similar to [22] but 3D magnet positioning combined with nonparallel rotational axes and independent magnet rotation improve the control output from 2D uniform fields to 3D fields and field gradients. Notably, this new system can be used to generate magnetic fields and forces in any direction with strengths comparable to or exceeding those of existing electromagnetic and permanent magnet systems. Each magnet rotates about its volumetric center, hence the new system contains no translating components and the rotational motion can be realized using inexpensive DC or stepper motors. These motors could be positioned an arbitrary distance away from the magnets in order to reduce the heat transferred from the motors to the workspace. A schematic image of the proposed system in shown in Fig. 1.

The system we propose is able to achieve or exceed many of the supposed advantages of electromagnetic devices while avoiding the problems normally attributed to permanent magnet systems. For example, the angular positions of the magnets can be set such that the field and field gradient have zero magnitude at any position in the workspace which is similar, from a control perspective, to the ability to turn off the field generated by an electromagnetic system. The permanent magnets generate a magnetic field without any heat production, which make the system particularly well suited for biomedical applications. The new magnetic actuation concept discussed in this paper was first reported in [23], but the work here includes an analysis of the control Jacobian as a metric for system fitness, more comprehensive field and force production demonstrations, and an optimization technique for selecting the system parameters that maximize the control capability.

The paper is structured as follows. A method for determining the control inputs for 5-DOF control using an arbitrary rotating magnet setup is outlined in Section II. Section III provides two methods to measure the control capability of a given magnet configuration, a brief summary of the number of actuator magnets required for control, and details regarding the prototype system that was constructed. Section IV contains experimental control demonstrations conducted using the prototype system. An optimization method is described in Section V with the purpose of designing systems for targeted applications.

II. CONTROL USING ROTATABLE PERMANENT MAGNETS

The untethered micro-device that is to be controlled is assumed to contain a permanent magnet with moment $\vec{m}_d$ and is located at position $\vec{p}$. The torque $\vec{T}$ exerted on this magnetic moment when subjected to an applied magnetic field with flux density $\vec{B}(\vec{p})$ at point $\vec{p}$ is given by

$$\vec{T} = \vec{m}_d \times \vec{B}(\vec{p}). \qquad (1)$$

This magnetic torque, when unopposed, will orient the magnetic moment in the direction of the applied magnetic
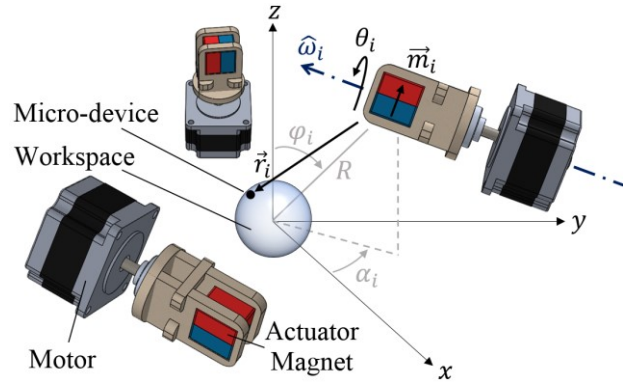

Fig. 1. Schematic image showing $N = 3$ actuator magnets, as well as the magnetic moment of the ith permanent magnet $\vec{m}_i$, the direction of which is defined by the motor spin angle θ_i about its rotational axis $\hat{\omega}_i$. The magnet center points are defined using spherical coordinates (R, α_i, φ_i). The position of the micro-device relative to the ith permanent magnet is denoted as $\vec{r}_i$.

field. For device applications in a liquid environment at low rotational speeds, the magnetic moment is able to quickly align with the field. In these cases, as long as the field magnitude is large enough to reject disturbances, the magnetic moment can be assumed to be always aligned with the field, and therefore the device heading can be controlled simply by adjusting the direction of the applied field. If the application requires precise torque regulation, the control method given in this paper can be reformulated to explicitly include the torque (similarly to the initial formulation in [3]), however, in many situations the pointing orientation of the device is sufficient.

The rotatable permanent magnets that are used for device actuation (henceforth referred to as actuator magnets) are approximated as point dipole sources located at the volumetric center of the magnets. The error associated with this approximation is less than 1% for cubic magnets located at least two side lengths from the workplace [24]. The magnetic field $\vec{B}$ at point $\vec{p}$ in the workplace is given by the linear addition of the fields from all N actuator magnets as

$$\vec{B}(\vec{p}) = \sum_{i=1}^{N} \frac{\mu_0 \|\vec{m}_i\|}{4\pi \|\vec{r}_i\|^3} (3\hat{r}_i \hat{r}_i^{\mathrm{T}} - I)\hat{m}_i \qquad (2)$$

where $\mu_0 = 4\pi \times 10^{-7}$ Tm·A^{-1} is the permeability of free-space, I is the 3×3 identity matrix, $\vec{r}_i$ is position of the micro-device relative to the center of the ith permanent magnet, $\vec{m}_i$ is the magnetic moment of the ith magnet, and $\hat{r}_i$ and $\hat{m}_i$ are the unit vectors of $\vec{r}_i$ and $\vec{m}_i$, respectively.

The actuator magnetic moment unit vector $\hat{m}_i$ can be parameterized by the rotational position of the ith magnet θ_i (henceforth referred to as motor angle) as

$$\hat{m}_i(\theta_i) = R_i[\cos(\theta_i) \quad \sin(\theta_i) \quad 0]^{\mathrm{T}} \qquad (3)$$

where R_i is a zy Euler angle rotation matrix defined by two rotation angles β_i and ξ_i, which correspond to rotations around the z and y axes, respectively.

The force exerted on the magnetic device with moment $\vec{m}_d$ at location $\vec{p}$ from the field gradients produced by the actuator magnets, assuming no current flowing in the workspace, is given by

$$\vec{F}(\vec{p},\vec{m}_d) = (\vec{m}_d \cdot \nabla)\vec{B}(\vec{p})$$

$$= \sum_{i=1}^{N} \left\{ \frac{3\mu_0 \|\vec{m}_i\|}{4\pi \|\vec{r}_i\|^4} \left(\hat{m}_i \hat{r}_i^{\mathrm{T}} + \hat{r}_i \hat{m}_i^{\mathrm{T}} - \left[5\hat{r}_i \hat{r}_i^{\mathrm{T}} - I \right]\left(\hat{m}_i \cdot \hat{r}_i \right) \right) \right\} \vec{m}_d.$$

(4)

In order to control a device with 5-DOF, the orientation and position of the device are adjusted by changing the magnetic field and force, respectively. As shown in (2) and (4), the field and force that are applied to the microrobot are a function of the magnetic moment direction $\hat{m}_i$ of each actuator magnet, which in turn varies with the motor angle θ_i as described in (3). Therefore the control inputs to the actuation system are the motor angles of all the actuator magnets $\vec{\theta} = \{\theta_1 \quad \theta_2 \quad ... \quad \theta_N\}^{\mathrm{T}}$. Due to the nonlinear relationship between the control inputs and the field and force outputs, linear algebra techniques cannot be used to determine the required control inputs as they can be with electromagnetic systems. Instead we find the control inputs as a solution to the nonlinear optimization problem

$$\min_{\vec{\theta}} \ f = K \left\| \vec{B}(\vec{\theta}) - \vec{B}_0 \right\|^2 + (1-K) \left\| \vec{F}(\vec{\theta}) - \vec{F}_0 \right\|^2 \quad (5)$$

where $\vec{B}_0$ and $\vec{F}_0$ are the desired field and force outputs, respectively; $\vec{B}(\vec{\theta})$ and $\vec{F}(\vec{\theta})$ are the field and force vectors that are produced for a given set of motor angles, respectively; and K is used to weigh the two halves of the equation to account for the difference in the units of measurement for the field and force, where $0 < K < 1$.

One method for choosing K involves the maximum field and force, denoted $B_{\max}$ and $F_{\max}$, respectively, that the system would be able to produce if the total magnetic volume of all N actuator magnets was concentrated at a single point R distance from the workspace center. Setting K equal to $(B_{\max})^{-2} / ((B_{\max})^{-2} + (F_{\max})^{-2})$ balances the field and force components of (5) based on the theoretical maximum system output. Depending on the relative importance of field and force generation in the desired application, K can be increased or decreased accordingly.

For an arbitrary permanent magnet configuration and arbitrary desired field and force vectors $\vec{B}_0$ and $\vec{F}_0$, the optimization problem given in (5) is non-convex with one or more local minima. Starting from an initial guess of the motor angles, the corresponding local minimum can be found using a gradient descent method. The gradient of (5) is given by

$$\frac{\partial f}{\partial \vec{\theta}} = 2 \begin{bmatrix} K\left(\vec{B}(\vec{\theta}) - \vec{B}_0\right)^{\mathrm{T}} & (1-K)\left(\vec{F}(\vec{\theta}) - \vec{F}_0\right)^{\mathrm{T}} \end{bmatrix} \begin{bmatrix} J_{\mathrm{B}}(\vec{\theta}) \\ J_{\mathrm{F}}(\vec{\theta}) \end{bmatrix}$$

(6)

where $J_{\mathrm{B}}(\vec{\theta})$ and $J_{\mathrm{F}}(\vec{\theta})$ are the rate Jacobians that locally relate a small change in motor angles to a small change in the field and force that are produced, respectively. Gradient descent iterations can be repeated from multiple starting points in order to find potentially superior local minima. As more local minima are found, the likelihood of finding a set of motor angles that exactly produce the desired field and force increases, however, for use in a feedback controller, control outputs are needed quickly to ensure control over the device is not lost, and therefore in general there will be insufficient time to find an arbitrarily small error for the motor angles. Instead, the search is halted once a reasonably accurate field and force are obtained. The acceptability of the result is determined by comparing the magnitude error and angle error between both $\vec{B}(\vec{\theta})$ and $\vec{B}_0$ as well as $\vec{F}(\vec{\theta})$ and $\vec{F}_0$ to a user-controlled threshold error value (in practice, several percent of the full magnitude and within a few degrees of the desired angle).

A further consideration for feedback control is that the field and force applied to the device will fluctuate as the magnets are rotated from one set of motor angles to the next. For systems using motors with limited speed, this phenomenon can have a large effect on the position and orientation of the device during these transitions. An effective way to reduce the change in motor angles is to begin the iterative gradient descent method for solving (5) using the motor angles from the previous control update. If that solution is not acceptable, other starting points near the previous set of motor angles can be considered subsequently. Additionally, the solution to (5) can be evaluated based on the magnitude of the change in motor angles in addition to the acceptability of the field and force that are produced.

III. DESIGN OF ACTUATOR MAGNET CONFIGURATION

A. Control Capability Metrics for System Optimization

There are a number of ways to quantify the control capabilities of an arbitrary configuration of actuator magnets depending on the application. The strength of the magnetic fields and forces that can be produced within the workspace is an important consideration for most applications. The ability to produce isotropic fields and forces ensures that control of the micro-device is not limited in some directions. The smallest singular value of the rate Jacobian relating motor angle speed to the time rate of change of the field and force output gives an approximate measure of the maximum motor rates required. More specific application-dependent system fitness measurements can be defined as well such as the region of uniform workspace size. In this paper, two separate fitness metrics will be considered for measurement and optimization of the control capabilities of a given magnet configuration: 1) a combined weighting of the

strength and isotropy of the force and field generation, and 2) the minimum singular value of the rate Jacobian.

The isotropy and strength of the fields and forces that a system is able to produce can be calculated based on the maximum field and force that can be generated in a number of sample directions. For each sample direction, the maximum field that the system can generate while simultaneously applying zero magnitude force is determined, as well as the maximum force that can be generated for a number of microrobot orientations while simultaneously applying a low strength field aligned with the microrobot heading. These maximum field and force samples are denoted $\vec{B}_{sp}$ and $\vec{F}_{sp}$, respectively. The strength of the field and force generation is taken as the average of the magnitudes from the corresponding sample. There is no simple formula to calculate isotropy for use as an optimization metric. The isotropy measurement must have some lower bound, corresponding to 0% isotropy, while 100% isotropy is achieved if every sampled magnitude is identical. Also, an isotropy measure that yields an intuitive result for the variance between vector magnitudes is desired. We designed an isotropy measure that is bounded between 0 and 1 and is approximately equal to one minus the average percent difference between the sample magnitudes and the mean of the sample magnitudes at higher values of isotropy. The formulation for the strength and isotropy of the field and force generation is given as

$$B_{str} = \text{AVG}\left(\vec{B}_{sp}\right), \quad F_{str} = \text{AVG}\left(\vec{F}_{sp}\right),$$

$$B_{iso} = \left(1 - \frac{SD\left(\vec{B}_{sp}\right)}{B_{str}\sqrt{\left\langle \vec{B}_{sp}\right\rangle - 1}}\right)^{1.6\left\langle \vec{B}_{sp}\right\rangle - 0.4}, \text{ and}$$

$$F_{iso} = \left(1 - \frac{SD\left(\vec{F}_{sp}\right)}{F_{str}\sqrt{\left\langle \vec{F}_{sp}\right\rangle - 1}}\right)^{1.6\left\langle \vec{F}_{sp}\right\rangle - 0.4}, \quad (7)$$

where for a vector $\vec{v}$, $\text{AVG}\left(\vec{v}\right)$, $SD\left(\vec{v}\right)$, and $\left\langle \vec{v}\right\rangle$ denote the mean, standard deviation, and number of elements of $\vec{v}$, respectively. One method to quantify the overall system fitness is as a weighted sum Q of these four metrics where

$$Q = C_1 B_{str} + C_2 B_{iso} + C_3 F_{str} + C_4 F_{iso}. \quad (8)$$

Another way to quantify the control capability is to consider the smallest singular value of the rate Jacobian. If the magnetic micro-device is assumed to be aligned with the field, (3) can be substituted into (2) and (4) to produce the nonlinear formula that gives the magnetic field and force as purely a function of the motor angles for a known arrangement of actuator magnets and micro-device location

$$\begin{bmatrix} \vec{B} \\ \vec{F} \end{bmatrix} = \begin{bmatrix} \vec{B}(\vec{\theta}) \\ \vec{F}(\vec{\theta}) \end{bmatrix} = \text{BF}(\vec{\theta}). \quad (9)$$

Taking the time derivative of (9) yields:

$$\begin{bmatrix} \dot{\vec{B}} \\ \dot{\vec{F}} \end{bmatrix} = \begin{bmatrix} J_{\text{B}}(\vec{\theta}) \\ J_{\text{F}}(\vec{\theta}) \end{bmatrix}\begin{bmatrix} \dot{\vec{\theta}} \end{bmatrix} = J_{\text{BF}}(\vec{\theta})\begin{bmatrix} \dot{\vec{\theta}} \end{bmatrix} \quad (10)$$

where $\dot{\vec{B}}$, $\dot{\vec{F}}$, and $\dot{\vec{\theta}}$, are the rate of change of the field, force, and motor angles, respectively, and J_{BF} is the $6 \times N$ Jacobian matrix computed by differentiating (9) with respect to $\vec{\theta}$. The Jacobian is a function of the fixed actuator magnet configuration, as well as the current state of the motor angles and micro-device position.

A full rank Jacobian at a specific motor angle state and micro-device position indicates that any desired change in field or force rate can be applied. Two distinct scenarios can cause the Jacobian to become rank deficient. The first occurs when the maximum field or force magnitude is already being applied and no motor velocity can increase the magnitude of the field/force any further (because the permanent magnet dipole magnitudes are fixed and the workspace separation distance R is constant). The second scenario occurs when the field and force strength are less than the maximum magnitude and yet some change in the field or force rate cannot be achieved, i.e. a control singularity. Ideally an arrangement of the magnets can be found such that the Jacobian is rank deficient only when the maximum field or force is being applied and therefore the system is capable of singularity-free control when being operated within its limits. For the analysis done in this paper, we will assume that the field and force are not at maximum strength and therefore any states where the Jacobian is not full rank are the result of the actuator magnet configuration.

The rank of the Jacobian at each state can be determined using a singular value decomposition; J_{BF} is full rank if the smallest singular value is larger than zero, although as the smallest singular value approaches zero, the required motor angle speed goes to infinity. The columns and rows of J_{BF} are scaled to produce a non-dimensional Jacobian $\tilde{J}_{\text{BF}}$ that maps changes in motor angle speed to non-dimensional changes in field and force per unit time

$$\tilde{J}_{\text{BF}}(\vec{\theta}) = \begin{bmatrix} \frac{1}{B_{\text{max}}}I & 0 \\ 0 & \frac{1}{F_{\text{max}}}I \end{bmatrix} J_{\text{BF}}(\vec{\theta}), \quad (11)$$

where I is the 3×3 identity matrix, and B_{max} and F_{max} are described in Section II. The non-dimensional Jacobian $\tilde{J}_{\text{BF}}$ has the same rank as J_{BF} and a singular value decomposition of $\tilde{J}_{\text{BF}}$ yields unit-consistent singular values [6]. The smallest unit-consistent singular value for a number of motor angle states and micro-device positions will also be used as a measure of system fitness. A larger minimum singular value results in a decrease in the maximum motor rotation speed that is required in worst-case control scenarios near singularities.

B. Minimum Number of Actuator Magnets

For electromagnetic coil systems with static magnetic sources, singularity-free control over the field and force applied on an untethered device requires eight coil inputs. The use of non-static magnetic control systems, such as the rotating magnet system presented here, reduces the number of required control inputs from eight to six [25]. A preliminary investigation into the control capability based on the number of actuator magnets supports this claim.

This investigation was conducted for setups with five, six, and eight magnets, and the system fitness was measured using the two methods described above. For each actuator magnet number, five randomly generated configurations were considered. Each configuration consisted of magnets equally spaced on a sphere but with random positions and random rotational axes. Despite the varying number of actuator magnets between setups, each of the configurations had a consistent workspace separation distance and the same total magnetic volume (equal to that of the prototype system described below). Representative fitness values for each actuator magnet number are given in Table I and are equal to the average fitness of the five randomly generated configurations. The system fitness measurements were made using 20 sample field directions, 144 sample force directions (for a micro-device with dipole moment of 10^{-6} Am^2 and variable heading) and 1500 combined motor angle states and micro-device positions for finding the minimum unit-consistent singular value.

The Jacobian for any configuration with $N \leq 5$ actuator magnets has fewer than six singular values, which means that singularity-free control of the field and force per unit time is never possible. Additionally, the $N = 5$ configurations were unable to produce a force in every sample direction, resulting in low force isotropy for these systems. The minimum singular value of the Jacobian for $N = 6$ and $N = 8$ configurations is non-zero (for the 1500 test cases), although the motor speeds required at some states may be undesirably high. A more rigorous examination of the minimum number of actuator magnets required for singularity-free control at every system state is ongoing work. The minimum singular value, as well as the strength and isotropy of the outputs increase with the number of actuator magnets from $N = 5$ to $N = 8$, but increasing N greater than eight does not result in substantial further improvements. An advantage, however, to using more actuator magnets is that the size of the solution set for a particular desired field and force is increased, i.e. a field and force can be generated using a larger number of different actuator motor angles. This additional solution space makes it easier to minimize the change in motor angles between control updates. Although six actuator magnets may be sufficient for full control, the prototype has been designed with eight magnets for better conditioned control capabilities and greatly reduced motor speed requirements for worst-case scenario control conditions.

TABLE I. PERFORMANCE COMPARISON FOR FIVE-, SIX- AND EIGHT-MAGNET SYSTEMS

	Number of Actuator Magnets		
	5	6	8
B_{str} (mT)	25.6	34.4	35.5
F_{str} (μN)	0.56	0.80	0.94
B_{iso} (%)	71.9	87.5	92.4
F_{iso} (%)	50.4	72.0	84.9
Smallest Singular Value	0	0.00001	0.0035

C. Prototype System

A prototype device was constructed in order to demonstrate the feasibility of using this type of magnetic

TABLE II: POSITIONS AND ROTATIONAL AXES DEFINED IN SPHERICAL COORDINATES FOR THE EIGHT ACTUATOR MAGNETS IN THE PROTOTYPE SYSTEM

Magnet	Positions (deg)		Rotational Axes (deg)	
	α	φ	β	ξ
1	335	115	70	60
2	40	105	225	145
3	235	112	315	20
4	90	45	148	235
5	198	45	265	260
6	305	55	25	225
7	70	180	275	90
8	166	115	350	130

actuation system to generate fields and forces for control of microrobots. The prototype has eight cubic magnets each with dipole moment $\|\vec{m}_i\| = 16.6$ Am^2, all positioned the same distance $R = 7.5$ cm from the center of the workspace. This combination of magnet strength and workspace distance was chosen as a compromise between maximizing the magnitude of the field and force generation while limiting the inter-magnetic torque that would have to be overcome by the motors, allowing for the components to be placed without physical interference, and ensuring a sufficient workspace separation to justify the dipole approximation which in this case has an error of less than 0.2% [24]. Since the workspace separation distance is the same for each of the eight actuator magnets, the positions and rotational axes can be more concisely defined using spherical coordinates: the azimuth and inclination angles for the magnet positions and rotational axes are denoted by (α, φ) and (β, ξ),

respectively, and are given in Table II. A photo of the prototype is shown in Fig. 2.

The prototype system was designed by manually varying the positions and rotational axes of the eight actuator magnets in order to improve the system fitness as described by (8). A moderately good system fitness was achieved despite a number of configuration constraints, most notably the limited motor placement positions that result from the simple structural pieces used to mount the motors to the base. The fitness metrics for the prototype device are B_{str} = 31.2 mT, F_{str} = 0.85 μN, B_{iso} = 90.7%, F_{iso} = 82.9%, and a minimum singular value of 0.003. A higher-performing system could be found using the more rigorous optimization method described in Section V.

For a spherical workspace of approximately 5 mm diameter, the field is uniform within 10% and 2° of the nominal magnitude and orientation, respectively, when a gradient of zero magnitude is requested. Non-zero gradients reduce the volume over which the field is uniform. For applications requiring a larger workspace, the position of the micro-device must be tracked in order to determine the field and force at the correct location. Magnetic interaction between actuator magnets also affects the performance of the system. Large inter-magnetic torques that result from closely positioned actuator magnets increase the likelihood that the motor torque will be overpowered and the motor will rotate away from its set point position (henceforth referred to as motor diversion). The maximum inter-magnetic torque between any two actuator magnets can be determined using (1) by considering the field produced by one magnet on the magnetic moment of the other magnet for every combination of the two motor angles. For any actuator magnet, this process can be repeated for each of the seven other magnets in the workspace and the sum of these seven inter-magnetic torques can be used to determine the upper bound on the total inter-magnetic torque that the corresponding motor will experience during operation. The highest total inter-magnetic torque for any motor in the prototype system is 0.34 Nm which necessitates running the motors at a fraction of their top speed to increase the mechanical torque output.

The permanent magnets used for the prototype system are transversely magnetized, grade N42 cubic NdFeB magnets with side length equal to 2.54 cm. Stepper motors of size NEMA 23 and capable of 0.39 Nm of stall torque were used to rotate the magnets at speeds up to 120 RPM. These motors have average capabilities and a future version of this system could be improved through the use of motors with higher torque and rotational speeds. Vibrations generated by the stepper motors are imperceptible using the feedback system but could be further reduced though the use of vibration damping mounts. The motors are controlled using motor driver boards (Quadstepper Motor Driver Board, SparkFun). Motor position feedback is obtained using magnetic rotary encoders (AS5040, ams AG). The driver boards and encoders were interfaced using a digital I/O

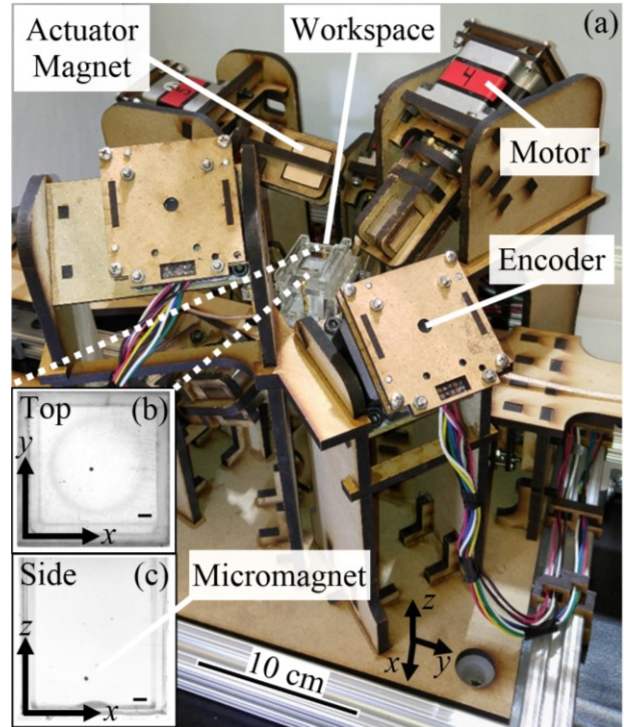board (USBDIO-48, Accessio) to a PC running Ubuntu Linux with custom control code.

Fig. 2. (a) Photo of the rotating magnet prototype system. (b), (c) camera views of the 250 μm micromagnet in the workspace with 1 mm scale bars. Video of the prototype during operation is available in the supplementary materials.

The structural pieces of the prototype were assembled using laser-cut pieces of high-density fiberboard. Two stationary cameras (FO134TC, Foculus) provide feedback from the top and side of the prototype. A detection algorithm was implemented for feedback control using a threshold function and Hough Transform using the openCV library, capable of detection at up to 60 fps. As a low-cost system, the total price of the prototype components (magnets, motors, motor drivers, encoders, and structural elements) is approximately 1000 USD. Additional components such as PC, DAQ card, and cameras cost about 2000 USD.

IV. SYSTEM CONTROL RESULTS

To demonstrate the capability of the prototype system, we test the static fields it can generate as well as perform several proof-of-concept field and force-application experiments including 1D open loop helical swimming, 2D feedback-controlled rolling path-following, and 3D feedback-controlled path following using gradient pulling.

The static field generation capability of the system is shown by requesting a 30 mT field in eight directions as well as a field of zero magnitude and comparing this desired field to the field produced by the system at the center of the workspace, measured using a single-axis gaussmeter (model 425, Lakeshore) in the *x, y,* and *z* directions. No specific magnetic field gradient was specified during this test. Table III shows the desired field, the average measured field for

two trials, the magnitude ratio of desired field to measured field, and the angle between the desired and measured field. The misalignment and magnitude difference between the desired field and measured field is small, less than 3.35° and 4.6%, respectively. These errors are likely due to fabrication and position errors in the laser-cut prototype frame since the errors predicted from the model are less than 0.09° and 0.3%. For increased accuracy, a calibration procedure to find the true magnet positions and rotation axes can reduce these

field magnitude no larger than 4×10^{-7} mT and a gradient smaller than 3×10^{-8} Tm^{-1} in every direction.

The ability to dynamically generate magnetic fields for micro-device control is demonstrated by two experiments. For the first, a helical, millimeter-scale swimmer was driven using a rotating field. The swimmer was assembled using a steel spring (length 6.4 mm, diameter 3 mm, period 1.3 mm) attached to a spherical NdFeB magnet head (diameter 1.9 mm) with magnetic moment oriented perpendicular to the

TABLE III: Comparison of the Measured Field to the Desired Field of 0 mT and 30 mT in Eight Different Directions

Test	1	2	3	4	5	6	7	8	9
$B_{desired}$ (mT)	$\begin{bmatrix} 0.00 \\ 0.00 \\ 0.00 \end{bmatrix}$	$\begin{bmatrix} 30.00 \\ 0.00 \\ 0.00 \end{bmatrix}$	$\begin{bmatrix} 0.00 \\ -30.00 \\ 0.00 \end{bmatrix}$	$\begin{bmatrix} 0.00 \\ 0.00 \\ 30.00 \end{bmatrix}$	$\begin{bmatrix} -21.21 \\ 21.21 \\ 0.00 \end{bmatrix}$	$\begin{bmatrix} 21.21 \\ 0.00 \\ -21.21 \end{bmatrix}$	$\begin{bmatrix} 0.00 \\ 21.21 \\ 21.21 \end{bmatrix}$	$\begin{bmatrix} -17.32 \\ -17.32 \\ -17.32 \end{bmatrix}$	$\begin{bmatrix} 17.32 \\ -17.32 \\ 17.32 \end{bmatrix}$
$B_{measured}$ (mT)	$\begin{bmatrix} 0.13 \\ -0.38 \\ 0.28 \end{bmatrix}$	$\begin{bmatrix} 30.38 \\ -0.44 \\ -0.76 \end{bmatrix}$	$\begin{bmatrix} -1.77 \\ -30.42 \\ 0.16 \end{bmatrix}$	$\begin{bmatrix} -0.95 \\ -0.01 \\ 30.09 \end{bmatrix}$	$\begin{bmatrix} -21.09 \\ 20.29 \\ 0.35 \end{bmatrix}$	$\begin{bmatrix} 22.68 \\ 0.68 \\ -21.79 \end{bmatrix}$	$\begin{bmatrix} 0.46 \\ 21.45 \\ 22.09 \end{bmatrix}$	$\begin{bmatrix} -17.94 \\ -17.59 \\ -18.00 \end{bmatrix}$	$\begin{bmatrix} 16.27 \\ -17.21 \\ 17.31 \end{bmatrix}$
$\dfrac{\lvert B_{desired}\rvert}{\lvert B_{measured}\rvert}$	-	0.987	0.985	0.997	1.025	0.954	0.974	0.971	1.023
$\angle$ (deg)	-	1.65	3.35	1.81	1.30	1.69	1.20	0.59	1.60

errors in future systems.

The static force production capability of the system is characterized by measuring the direction of the Cartesian velocity of a small magnetic device as it is subjected to a desired force. The device used for this test is a cubic NdFeB magnet with side length equal to 250 µm (henceforth referred to as the micromagnet) and the test is conducted in a horizontal container filled with silicone oil with a viscosity of 350 cSt. The micromagnet is maneuvered to the center of the horizontal workspace and then held stationary by applying a zero force. Once stationary, a set of motor angles is found that result in a desired force direction and magnitude. After the motors have completed the rotation to the set of motor angles, the velocity direction of the micromagnet over time is measured and compared to the requested force direction. Three different force directions were tested (*x, y,* and *xy*) and the angle difference between the desired direction and actual direction, averaged over five trials per requested direction, was found to be 4.6°, 5.2°, and 5.3°, respectively. The speed of the micromagnet during each experiment varies between trials, an effect likely due to changing friction and viscous drag from dragging the magnet along the bottom of the container.

The system's ability to simultaneously produce zero magnitude fields and field gradients was determined in simulation. Fifteen distinct workspace positions were considered: the workspace center and 14 equally spaced points on a sphere of radius 5 mm. At each of the 15 positions a set of motor angles was found that resulted in a
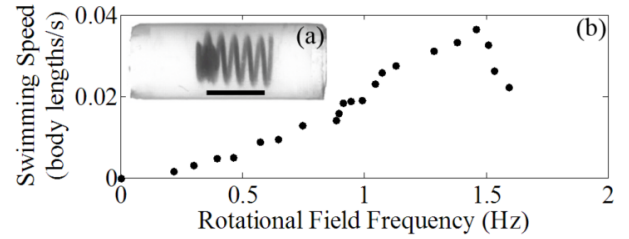

Fig. 3. (a) Image of the helical swimmer used to demonstrate rotational field production capability and 5 mm scale bar. (b) Swimmer speed as function of applied field frequency from 0 to 1.6 Hz.

spring axis. The helical swimmer was immersed in 350 cSt viscosity silicone oil inside a tube with inner diameter 4.1 mm. A rotational field was applied in the plane perpendicular to the tube axis causing the swimmer to rotate and screw through the liquid. A magnetic force of zero magnitude was requested during the experiment, assuming that the dipole moment of the swimmer was aligned with the applied field (an assumption which is accurate for low rotation rates but could introduce errors when the rotation rate increases).

The linear speed of the swimmer was measured for field rotation frequencies of 0 to 1.6 Hz, as shown in Fig. 3. As the frequency is increased, the direction of the swimmer's dipole moment increasingly lags behind the rotating field until the step-out point where the lag reaches 90° and the swimmer falls out of synchronization with the applied field [26]. The purpose of this simple demonstration is to show that a rotating field can be generated over a range of

frequencies to produce the expected linear change in swimmer velocity prior to reaching the step-out frequency, which in this case is roughly 1.4 Hz. For applied field frequencies less than 1.4 Hz, the swimming speed increases with frequency at approximately 0.02 body lengths per second times the frequency in hertz, although the relationship is not exactly linear possibly due to intermittent contact between the swimmer and the tube wall or the non-zero magnetic forces that are produced as the swimmer becomes desynchronized with the applied field. The maximum rotating field frequency that the prototype system is able to generate is around 1.6 Hz while a highly engineered system with high torque, DC motors would be capable of producing rotational fields with frequency greater than 100 Hz.

The second proof of concept experiment involved rolling a micromagnet in a 2D path-following demonstration by applying rotational fields. During the experiment, a magnetic force of zero magnitude was requested, assuming the microdevice dipole was always aligned with the rotating field. For a triangular-shaped path of approximately 10 mm in length, the average path deviation and speed for five trials was 102 μm and 149 μm·s^{-1}, respectively. The rotation frequency of the applied field was around 0.2 Hz. A video of this experiment can be found in the supplementary materials.

To demonstrate the dynamic force generation capabilities of the prototype, a 3D feedback control experiment was conducted. The task was to pull the 250 μm micromagnet along a predetermined path defined by seven goal points using magnetic forces. The position of the micromagnet was obtained from the top and side-view cameras at a rate of 60 Hz. The required change in motor angles at each control update was reduced by limiting the change between consecutive desired force vectors. For example, the large change in desired force vector direction after a goal point was reached would require a large change in motor angles. Instead, the desired force was decreased to zero as each goal was approached, then increased in the direction of the next goal point. This approach reduced the average change in motor angle between control updates to less than three degrees. In addition, a constant, vertical, magnetic force offset was applied to counteract the weight of the micro-device. The magnitude of this vertical offset force was found by driving the micro-device to the center of the workspace and manually tuning the gain value until there was no vertical motion. To orient the micromagnet, the requested field was held constant in magnitude (7 mT) and direction but was allowed to vary by 5 mT and 12° in order to increase the speed of finding a suitable solution to (5) in the shortest amount of time. Using our simple gradient-descent search algorithm, the average computation time for one control update was 0.001 s.

The direction of the requested force during each control update is determined using a simple path following algorithm. The desired force is chosen such that the micro-device is driven along the path towards to the next goal point

and perpendicularly back to the path to reduce the deviation error. The direction is given by

$$\hat{d}_F = (1-K_1)K_2 \cdot \hat{d}_G + K_1(1-K_2) \cdot \hat{d}_P \qquad (12)$$

where $\hat{d}_F$ is a unit vector in the direction of the desired force; $\hat{d}_G$ is a unit vector in the direction of the next goal point; $\hat{d}_P$ is a unit vector from the micromagnet back to the path; K_1 is gain value that increases as the perpendicular distance from the micromagnet to the path increases, $0 < K_1 < 1$; and K_2 is a gain value that can be used to tune the relative amount of path following, $0 < K_2 < 1$. The magnitude of the desired force can also be modified to affect the micromagnet motion. In order to tune the values of K_2 and the desired force magnitude, multiple trials of a short 3D
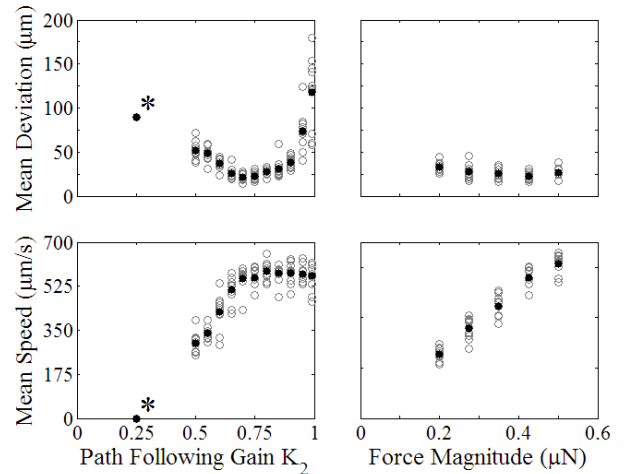

Fig. 4. Path deviation and speed as a function of desired force magnitude and path following gain K_2 for gradient pulling of a micromagnet in 3D. The results for ten trials of each parameter value are shown as open circles along with the average of the ten trials with filled circles. Points marked by * represent a single trial. This analysis omits any section of the trials during which a motor diverted.

path were completed using a range of gain parameters. During these trials, the average micromagnet path deviation and speed along the path, defined as the perpendicular distance between the agent and the path, and the path length divided by the completion time, respectively, were analyzed.

For 3D path following, random instances of motor diversion, as described in Section III, can cause a large deviation of the micromagnet from the path. After the motor diversion is detected by the encoder, the motor will be driven back to its set point and the micromagnet will return to the path, however, the deviation during this interval can be quite large compared to the rest of the trial. The large path deviations that result from randomly occurring motor diversions (which, for identical trial parameters, may occur multiple times in a single trial or not at all) can produce wildly varying average path deviations and path speeds between trials despite identical gain values. Therefore in order to determine a clear relationship between the gain parameters and the path deviation and speed, any portion of

each trial in which a motor diverted was omitted from the analysis. The results of this experiment are shown in Fig. 4.

As the K_2 gain is decreased from a value of 1, path following is weighed more heavily over waypoint following and the average deviation decreases. At K_2 values lower than 0.7, however, the micromagnet starts to overshoot the path resulting in an increase in average deviation and a decrease in path speed. For values of K_2 much smaller than 0.5, the motor speed is not fast enough to achieve the rapid changes in desired force direction and the micromagnet oscillates around the path making no progress. Additionally, the incidence of motor diversion increases as K_2 is decreased; this result is omitted from this set of tests but will have an effect on the comprehensive path following results given below. The magnitude of the desired force has a negligible effect on the path deviation but shows an approximately linear relationship with path speed. The results indicate that choosing K_2 to be 0.7 and a force magnitude value of 0.5 µN will produce results with minimal deviation and the quickest path speed.

For the full 3D path following demonstration, the path deviation and speed were determined for the entirety of each trial even in the presence of motor diversion. Path following was conducted using two different silicone oil viscosities: 350 cSt and 1000 cSt. In the 350 cSt trials, instances of motor diversion can cause large path deviations and therefore the K_2 gain was set at 0.85 to reduce the diversion frequency. The average deviation across ten trials was 38 µm and the average velocity 580 µm·s⁻¹. In the 1000 cSt trials, motor diversion causes smaller deviations so the K_2 gain was set at 0.7. The average deviation across ten trials was 25 µm and the average velocity 310 µm·s⁻¹. The outcome of a typical feedback control test conducted in 1000 cSt silicone oil is shown in Fig. 5. The average deviation for this single trial is 22 µm.

V. SYSTEM PARAMETER OPTIMIZATION RESULTS

A. General Considerations for System Optimization

The experimental results shown above demonstrate that the prototype system is capable of producing fields and forces for a variety of control applications. In the final section of this paper we present an optimization framework that can be used to design rotating magnet systems for more specialized applications. We consider the optimization of two separate fitness metrics: the combined strength and isotropy of the field and force production given in (8), and the minimum unit-consistent singular value of the normalized Jacobian given in (11). We also present optimization results for a system with highly constrained magnet positions representing an application where the actuator space is largely inaccessible.

In an optimization of the system control capability, potential choices for the optimization variables include the positions of the centers of the actuator magnets, the direction

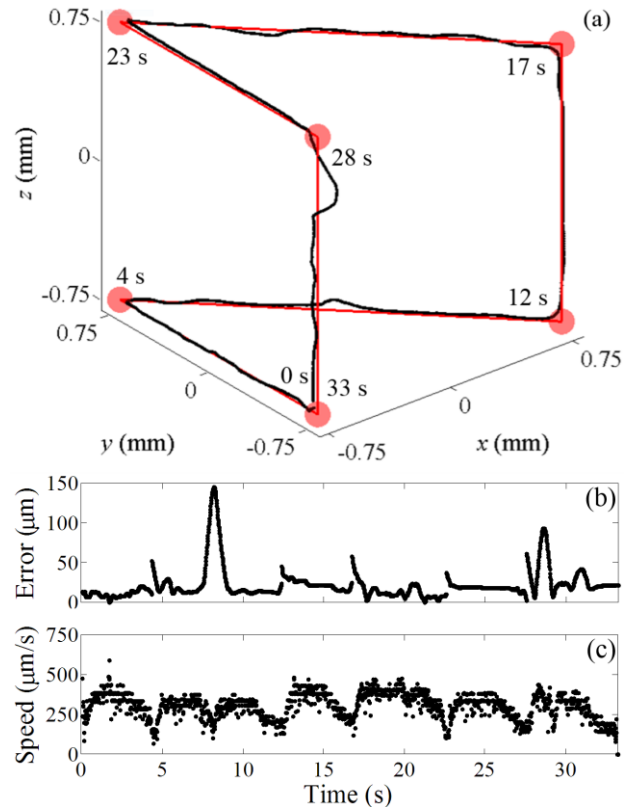of the rotational axes of the magnets, the number of magnets, and the magnitude of the dipole moments of the

Fig. 5. A typical feedback result for a 250 µm magnet performing path following in the three dimensions. The micromagnet position has been low-pass filtered. (a) Path of the micromagnet in black and the goal points and desired path in red. Elapsed time at each goal point is indicated. The micromagnet deviation from the path (b) and speed (c).

magnets, which is proportional to the magnet volume. The field and force produced by each magnet scale linearly with the dipole moment as given in (2) and (4), respectively, and therefore any increase in dipole moment magnitude will result in an increase in field and force strength. In practice, however, the dipole moment will be limited by the size of the actuator magnets that are available. Also, the non-dimensional Jacobian is normalized using the B_{max} and F_{max} terms as shown in (11), so for setups with actuator magnets that have equal dipole moments the minimum unit-consistent singular value is independent of the dipole magnitude. The relationship between control capability and the number of actuator magnets was analyzed in Section III. Therefore, optimization results discussed hereafter will be for a fixed number of magnets and fixed dipole moment magnitudes but variable magnet positions and rotational axes.

A major consideration for this optimization is the large remaining parameter search space. The position and rotational axis of each actuator magnet can be defined using three and two parameters, respectively, for a total of five variables per magnet. Placing the magnets closer to the workspace increases the magnitude of the field and force

generation, as described in (2) and (4), respectively. If all the magnets are placed at a minimum separation distance from the workspace, necessitated by the physical workspace constraints and the dipole approximation spacing, each magnet position can be defined using two spherical coordinates reducing the number of variables from five to four. This constraint was implemented for the optimization trials resulting in a search space for an eight magnet configuration with 32 dimensions.

The optimization trials were performed using the MATLAB *fminsearch* algorithm. This algorithm uses the Nelder-Mead simplex method which is inefficient when optimizing over a large number of variables [27]. One way to reduce the search complexity is to use a coordinate descent algorithm to iteratively optimize over a smaller search space until convergence is achieved for the full optimization problem. In practice this was done by optimizing over the four free parameters of a single magnet at one time while holding the parameters of the other seven magnets constant (hereafter referred to as a coordinate descent iteration). A coordinate descent iteration was performed for each of the eight magnets in sequence repeatedly until convergence was reached. This method has similar convergence properties to a steepest descent algorithm performed over all the variables simultaneously [28] and therefore is suitable for finding a local optimal solution near the starting configuration. Due to the nonlinearity of the fitness functions and the large search space, it is unlikely that the global solution will be found, so the search is ended when a local optimum is reached. Four non-optimized system configurations were considered as the initial setups for the optimizations. These initial setups include: 1. prototype system; 2. magnet centers equally spaced on cube vertices; 3. magnet centers randomly positioned by equally spaced; 4. magnet centers arbitrarily positioned. The initial rotational axes for setups 2, 3, and 4 were arbitrarily selected. Three-dimensional views of the initial and optimized configurations are shown in the supplementary video.

B. Maximizing Combined Field and Force Strength and Isotropy

For system applications requiring large magnetic fields and forces, one way to design a suitable rotating magnet system is to optimize the system parameters in order to maximize the weighted sum of the strength and isotropy of the field and force production given by (8). Although (8) can be optimized using the *fminsearch* function, it requires the maximum force to be sampled for many different robot headings to form the $\vec{F}_{sp}$ vector and this step represents the majority of the calculation time required to measure the fitness. The total optimization time can be greatly reduced if $\vec{F}_{sp}$ is not calculated at all and the system fitness is calculated solely on the ability to produce strong and isotropic fields by considering only the portion of the total system fitness given in the objective function

$$Q_B = C_1 B_{str} + C_2 B_{iso}. \quad (13)$$

The authors have found that in most of the cases analyzed, as the field production capabilities are improved, so too are the force production capabilities. In other words, optimizing the fitness of a system as given by (13) usually improves the isotropy and strength of both the fields and forces that can be generated.

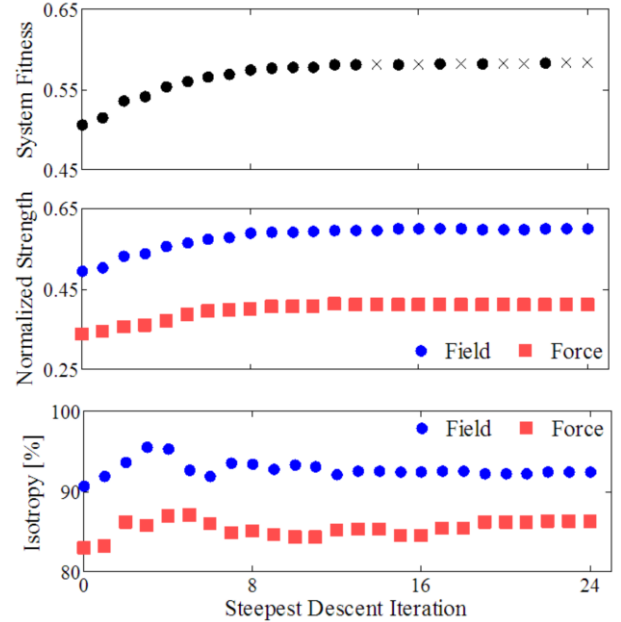The objective function given in (13) was calculated using

Fig. 6. System fitness values at the conclusion of each coordinate descent iteration during the optimization starting from the prototype system parameters. The × symbol represents instances where the optimization failed to find an improvement in total system fitness. The field and force strength have been normalized as a percentage of the maximum field and force that can be produced by the total actuator magnetic volume placed at a single point R distance from the workspace.

10 representative field samples which are indicative of the system's ability to produce a field in every direction. To

TABLE IV. STRENGTH AND ISOTROPY OF CONTROL OUTPUTS PRE- AND POST-OPTIMIZATION OF THE SYSTEM PARAMETERS

		Starting Configuration			
		1	2	3	4
Q	Initial	0.507	0.446	0.547	0.448
	Final	0.584	0.583	0.588	0.588
B_{str} (mT)	Initial	31.2	26.4	35.3	25.7
	Final	37.9	37.6	38.2	38.2
F_{str} (μN)	Initial	0.85	0.74	0.90	0.77
	Final	1.03	1.04	1.02	1.02
B_{iso} (%)	Initial	90.7	81.7	95.9	87.7
	Final	92.5	90.7	95.8	96.3
F_{iso} (%)	Initial	82.9	79.7	84.2	74.8
	Final	86.3	88.4	87.9	87.6

ensure that the system fitness given by (8) was monotonically increasing during the optimization of (13), a more thorough check of the total system fitness was completed using 20 sample field directions and 144 combined force and microrobot orientation directions after each coordinate descent iteration. In instances where the total system fitness failed to increase after a coordinate descent iteration, this configuration change was discarded and the optimization continued using the parameters of the next magnet in the sequence. The optimization was considered to have reached convergence once the total fitness failed to increase for five of the eight coordinate descent iterations in a given sequence. The system fitness, normalized field and force strengths, and field and force isotropies are shown in Fig. 6 for each coordinate descent iteration starting from the prototype configuration. The numerical values of the system fitness components before and after the optimization are given in Table IV for the four starting configurations that were considered. The field and force strength are improved by approximately 10 to 50% depending on the initial fitness values while the isotropy increase is capped at about ten percentage points.

In situations where the desired application requires strict constraints on the system parameters, the optimization technique described above has the ability to find non-intuitive setups with relatively high fitness that are not likely to be found through manual manipulation of the system parameters. As an example of an extreme case, consider constraining the azimuth angle of the magnet centers to be between 0° and 90° (i.e. a bird's eye view of the setup would show all magnets placed in the first quadrant). The initial configuration had actuator magnets evenly spaced within the first quadrant. Performing the automated optimization with this constraint yielded a system with fitness components given in Table V. The system fitness improvement is larger than the non-constrained cases above, especially for the field and force strength which both increase by more than 60%. The control capabilities of this highly constrained system are approximately equal to those of the prototype system despite the extreme limitation on the magnet positions. This result also demonstrates the rotating magnet system concept presented in this paper has the ability to achieve a high level of control in applications where a significant portion of the actuator space is inaccessible.

C. Maximizing Minimum Singular Value

For system applications in which the maximum motor speed is a more important consideration compared to the field and force strength, the system parameters can be optimized in order to increase the minimum unit-consistent singular value of the non-dimension Jacobian $\widetilde{J}_{BF}$ given in (11) in order to reduce the maximum motor rates required during operation. The smallest singular value was calculated for 100 motor angle states at 15 micromagnet locations consisting of the workspace center as well as 14 equally spaced points that define a sphere of radius 5 mm. The

TABLE V. STRENGTH AND ISOTROPY OF CONTROL OUTPUTS PRE- AND POST-OPTIMIZATION FOR HIGHLY CONSTRAINED SYSTEM PARAMETERS

	Constrained Optimization		Prototype System
	Initial	Final	
Q	0.334	0.501	0.507
B_{str} (mT)	15.5	31.3	31.2
F_{str} (μN)	0.51	0.84	0.85
B_{iso} (%)	80.7	88.7	90.7
F_{iso} (%)	73.8	81.6	82.9

optimization metric was taken as the smallest minimum singular value from these 1500 states. The coordinate descent method described above was used to optimize over the parameters of each of the magnets individually in order to reduce the size of the search space. A non-constrained optimization was performed on the same four initial setups as in the previous set of tests. The minimum unit-consistent singular values for the systems before and after the optimization are shown in Table VI. The minimum singular values are improved by a factor of roughly 1.5 to 4.

The corresponding decrease in required motor angular rates for this increase in minimum singular value is found

TABLE VI. MINIMUM SINGULAR VALUE PRE- AND POST-OPTIMIZATION OF THE SYSTEM PARAMETERS

		Starting Configuration			
		1	2	3	4
Minimum Singular Value	Initial	0.003	0.002	0.007	0.002
	Final	0.013	0.007	0.011	0.007

using the following method. The pseudoinverse of $\widetilde{J}_{BF}$ can be used to find the motor speeds that are required to produce a desired non-dimensional field and force per unit time. Using the pseudoinverse of $\widetilde{J}_{BF}$, the maximum motor angle rate required for a unit magnitude field and force rate was calculated for a number of system states and compared to the minimum singular value of $\widetilde{J}_{BF}$ at each state. This analysis showed that the maximum required motor speed roughly scales with the reciprocal of the minimum singular value. Therefore improving the minimum singular value by a factor of approximately 1.5 to 4 results in a decrease of the maximum required motor speed by roughly 40 to 70% in worst-case scenarios near singularities.

The manually designed prototype system described in this paper is able to make moderately high-strength fields and forces in order to accomplish a number of general magnetic actuation tasks. For applications with more specific control

requirements, a system with a high level of performance can be designed by optimizing the desired system fitness metric. The optimization method presented has been shown to be capable of making meaningful improvements for two specific optimization targets: 1) increasing the field and force strength for field and gradient limited applications and 2) improving the minimum unit-consistent singular value of the normalized Jacobian to reduce the maximum motor rate required during operation.

VI. CONCLUSIONS

In this work we have shown the capability for a novel permanent-magnet actuation system to achieve an equivalent level of control to electromagnetic systems for the motion of untethered micro-scale magnetic devices. We have shown the unexpected result that this permanent magnet system is able to produce zero magnitude fields and gradients in the workspace. We show that the magnet configuration can be optimized for a high level of control even in the presence of strict constraints on the positions of the magnets, which motivates the use of this system for applications with limited actuator space. While this type of magnetic actuation may struggle with tasks requiring the use of high frequency or uniform magnetic fields, as well as situations where the field must be turned off over the entire space around the system, this magnetic actuation method is particularly capable for heat-sensitive procedures requiring strong magnetic fields and forces for full 5-DOF control. Potential applications include laboratory experiments such as the manipulation of single cells as well as medical procedures involving larger magnetic implements such as capsule endoscopes and steerable needles.

ACKNOWLEDGMENT

REFERENCES

[1] E. Diller and M. Sitti, "Micro-scale mobile robotics," *Foundations and Trends in Robotics*, vol. 2, no. 3, pp. 143–259, 2013.

[2] B. J. Nelson, I. K Kaliakatsos, and J.J. Abbott, "Microrobots for minimally invasive medicine," *Annual Review of Biomedical Engineering*, vol. 12, pp. 55–85, 2010.

[3] M. P. Kummer, J. J. Abbott, B. E. Kratochvil, R. Borer, A. Sengul, and B. J. Nelson, "Octomag: An electromagnetic system for 5-DOF wireless micromanipulation," *IEEE Transactions on Robotics*, vol. 26, no. 6, pp. 1006–1017, 2010.

[4] F. Carpi and C. Pappone, "Stereotaxis niobe magnetic navigation system for endocardial catheter ablation and gastrointestinal capsule endoscopy," *Expert Review of Medical Devices*, vol. 6, no. 5, pp. 487–498, 2009.

[5] F. P. Gosselin, V. Lalande, S. Martel, "Characterization of the deflections of a catheter steered using a magnetic resonance imaging system," *Medical Physics*, vol. 38, no. 9, pp. 4994–5002, 2011.

[6] A. W. Mahoney and J. J. Abbott, "Five-degree-of-freedom manipulation of an untethered magnetic device in fluid using a single permanent magnet with application in stomach capsule endoscopy,"

[7] P. Valdastri, M. Simi, and R. J. Webster III, "Advanced technologies for gastrointestinal endoscopy," *Annual Review of Biomedical Engineering*, vol. 14, pp. 297–429, 2012.

[8] E. B. Steager, M.S. Sakar, C. Magee, M. Kennedy, A. Cowley, and V. Kumar, "Automated biomanipulation of single cells using magnetic microrobots," *The International Journal of Robotics Research,* vol. 32, no. 3, pp. 346–359, 2013.

[9] I. S. M. Khalil, L. Abelmann, and S. Misra, "Magnetic-based motion control of paramagnetic microparticles with disturbance compensation," *IEEE Transactions on Magnetics,* vol. 50, no. 10, pp. 1–10, 2014.

[10] J. Keller, A. Juloski, H. Kawano, M. Bechtold, A. Kimura, H. Takizawa, and R. Kuth, "Method for navigation and control of a magnetically guided capsule endoscope in the human stomach," *IEEE Int. Conf. on Biomedical Robotics and Biomechatronics*, pp. 859–865, 2012.

[11] E. Diller, J. Giltinan, G. Lum, Z. Ye, and M. Sitti, "Six-degree-of-freedom magnetic actuation for wireless microrobotics," *International Journal of Robotics Research*, vol. 35, no. 1, pp. 114–128, 2016.

[12] E. Diller, J. Giltinan, and M. Sitti, "Independent control of multiple magnetic microrobots in three dimensions," *The International Journal of Robotics Research*, vol. 32, no. 5, pp. 614–631, 2013.

[13] S. Chowdhury, W. Jing, and D. J. Cappelleri, "Controlling multiple microrobots: recent progress and future challenges," *Journal of Micro-Bio Robotics*, vol. 10, pp. 1–11, 2015.

[14] S. Erni, S. Schürle, A. Fakhraee, B. E. Kratochvil, and B. J. Nelson, "Comparison, optimization, and limitations of magnetic manipulation systems," *Journal of Micro-Bio Robotics*, vol. 8, no. 3-4, pp. 107–120, 2013.

[15] D. R. Frutiger, K. Vollmers, B. E. Kratochvil, and B. J. Nelson, "Small, fast, and under control: wireless resonant magnetic micro-agents," *The International Journal of Robotics Research*, vol. 29, no. 5, pp. 613–636, 2010.

[16] C. Pawashe, S. Floyd, and M. Sitti, "Modeling and experimental characterization of an untethered magnetic micro-robot," *The International Journal of Robotics Research*, vol. 28, no. 8, pp. 1077–1094, 2009.

[17] T. W. Fountain, P. V. Kailat, and J. J. Abbott, "Wireless control of magnetic helical microrobots using a rotating-permanent-magnet manipulator," *IEEE Int. Conf. on Robotics and Automation*, pp. 576–581, 2010.

[18] A. W. Mahoney and J. J. Abbott, "Generating rotating magnetic fields with a single permanent magnet for propulsion of untethered magnetic devices in a lumen," *IEEE Transactions on Robotics*, vol. 30, no. 2, pp. 411–420, 2014.

[19] G. Lien, C. Liu, J. Jiang, C. Chuang, and M. Teng, "Magnetic control system targeted for capsule endoscopic operations in the stomach—design, fabrication, and in vitro and ex vivo evaluations," *IEEE Transactions on Biomedical Engineering*, vol. 59, no. 7, pp. 2068–2079, 2012.

[20] S. Yim and M. Sitti, "Design and rolling locomotion of a magnetically actuated soft capsule endoscope," *IEEE Transactions on Robotics*, vol. 28, no. 1, pp. 183–194, 2012.

[21] G. Ciuti, P. Valdastri, A. Menciassi, and P. Dario, "Robotic magnetic steering and locomotion of capsule endoscope for diagnostic and surgical endoluminal procedures," *Robotica*, vol. 28, no. 2, pp. 199–207, 2010.

[22] W. Zhang, Y. Meng, and P. Huang, "A novel method of arraying permanent magnets circumferentially to generate a rotation magnetic field," *IEEE Transactions on Magnetics*, vol. 44, no. 10, pp. 2367–2372, 2008.

[23] P. Ryan and E. Diller, "Five-degree-of-freedom magnetic control of micro-robots using rotating permanent magnets," *IEEE Int. Conf. on Robotics and Automation*, 2016.

[24] A. J. Petruska and J. J. Abbott, "Optimal permanent-magnet geometries for dipole field approximation," *IEEE Transactions on Magnetics*, vol. 49, no. 2, pp. 811–819, 2013.

[25] A. J. Petruska, and B. J. Nelson, "Minimum bounds on the number of electromagnets required for remote magnetic manipulation," *IEEE Transactions on Robotics*, vol. 31, no. 3, pp. 714–722, 2015.

[26] K. Ishiyama, K. I. Arai, M. Sendoh, and A. Yamazaki, "Spiral-type micro-machine for medical applications," *Journal of Micromechatronics,* vol. 2, no. 1, pp. 77–86, 2002.

[27] F. Gao, and L. Han, "Implementing the Nelder-Mead simplex algorithm with adaptive parameters", *Computational Optimization and Applications,* vol. 51, no. 1, pp. 259–277, 2012.

[28] D. Bertsekas, "Unconstrained optimization," in *Nonlinear Programming*, 2nd ed., Belmont, MA: Athena Scientific, ch. 1, sec. 1.82, pp.161, 1999.

Patrick Ryan received the B.S. degree in mechanical engineering from Queens University in 2014 and the M.A.Sc. degree in mechanical engineering from the University of Toronto, in 2016. He is currently working as an R&D Engineer in industry with research interests in mechatronics and medical systems.

Eric Diller received the B.S. and M.S. degree in mechanical engineering from Case Western Reserve University in 2010 and the Ph.D. degree in mechanical engineering from the Carnegie Mellon University in 2013. He is currently Assistant Professor in the department of Mechanical and Industrial Engineering at the University of Toronto, where he is director of the Microrobotics Laboratory. His research interests include micro-scale robotics and bio-inspired novel locomotion systems, and features fabrication and control relating to remote actuation of micro-scale devices using magnetic fields, micro-scale robotic manipulation, smart materials.

He is an Associate Editor of IEEE Robotics and Automation Letters and the Journal of Micro-Bio Robotics. He received the award for Best Associate Editor at the 2015 IEEE International Conference on Automation and Robotics, and the Connaught New Researcher Award and the Ontario Early Researcher Award in 2017.